Proc. VII Symp. on Crystallisation in Glasses and Liquids, Sheffield, 6–9 July 2003 *Phys. Chem. Glasses*, 2004, **45**, 107–115

Nucleation and polycrystalline solidification in binary phase field theory

L. Gránásy,[1] *T. Pusztai, T. Börzsönyi*

Research Institute for Solid State Physics and Optics, H-1525 Budapest, POB 49, Hungary

J. A. Warren

Metallurgy Division, National Institute of Standards and Technology, Gaithersburg, Maryland 20899, USA

B. Kvamme

University of Bergen, Department of Physics, Allégaten 55, N-5007 Bergen, Norway

P. F. James

Glass Research Centre, Department of Engineering Materials, The University of Sheffield, Sir Robert Hadfield Building, Mappin Street, Sheffield S1 3JD, UK

We present a phase field theory for the nucleation and growth of one and two phase crystals solidifying with different crystallographic orientations in binary alloys. The accuracy of the model is tested for crystal nucleation in single component systems. It is shown that without adjustable parameters the height of the nucleation barrier is predicted with reasonable accuracy. The kinetics of primary solidification is investigated as a function of model parameters under equiaxial conditions. Finally, we study the formation of polycrystalline growth morphologies (disordered dendrites, spherulites and fractal-like aggregates).

Polycrystalline solidification is of general interest from both practical and theoretical viewpoints. To describe such a process we need a model that can handle crystal nucleation and growth on equal footing. Over the past decade the phase field theory (PFT) has demonstrated its ability to describe complex solidification morphologies(1) including thermal and solutal dendrites(2–7) and eutectic/peritectic fronts.(8–11) In the PFT, nucleation has been modelled by introducing Langevin noise into the governing equations(9,12) or by inserting supercritical particles into the simulation window.(11,13) Until recently,(14–18) differences in the crystallographic orientation of the nucleating/growing particles could not been handled. In this paper we present results on modelling polycrystalline morphologies achieved by extending the approach of Kobayashi, Warren & Carter (KWC).(14) KWC introduced a normalised orientation angle that describes the orientation of the crystal planes in the laboratory frame. In our approach, developed recently,(15–17) the orientation is now extended to the liquid to describe local order in that phase. This allows us to handle such processes as freezing of orientation defects and grain boundaries into the solid, while taking the respective free energy penalties into account. Here we demonstrate that the formation of a broad range of polycrystalline morphologies can be addressed within the framework of this approach.

In this paper, first we apply the phase field theory for describing crystal nucleation in undercooled liquids. We test the accuracy of the predictions for one and two component systems (Lennard–Jones, ice water, hard sphere and the nearly ideal solution Cu–Ni). Then we present a phase field theory that handles the nucleation and growth of crystallites with different crystallographic orientations. It is applied to study crystallisation kinetics in binary two-dimensional liquids. In the last part of our paper, various polycrystalline morphologies are presented that can be described using our approach.

Phase field theory for nucleation

Our starting point is the standard phase field theory of binary alloys as developed by several authors.(5,19) The Helmholtz free energy is a functional of two fields. 1. A nonconservative a structural order parameter, φ, that describes the local crystallinity of the matter. (Nonconservative means that its volume integral is not conserved.) This quantity can be viewed as the Fourier amplitude of the dominant density wave of the time averaged singlet density in the solid. As pointed out by Shen & Oxtoby(20) if the density peaks in the solid can be well approximated by Gaussians placed to the atomic sites, all Fourier amplitudes can be expressed uniquely in terms of the amplitude of the dominant wave, thus a single structural order parameter suffices. Here we take φ=0 in the solid and φ=1 in the liquid.

---

[1] Corresponding author. Email: grana@szfki.hu

2. The concentration (solute) field, c. We assume mass conservation which implies that the integral over volume of this field is a constant.

In terms of these fields, the free energy functional is written in the following form

$$F=\int d^3r\left\{\frac{1}{2}\varepsilon_\varphi^2 T\Gamma(\nabla\varphi)^2+f(\varphi,c)\right\} \tag{1}$$

where in the case of isotropic systems, $\Gamma(\nabla\varphi)^2=(\nabla\varphi)^2$, ε_φ is a constant, T the temperature and $f(\varphi,c)$ the local free energy density. The first term on the right hand side is responsible for the appearance of the diffuse interface. The local free energy contribution has the form $f(\varphi,c)=[(1-c)w_A+cw_B]Tg(\varphi)+[1-p(\varphi)]f_S+p(\varphi)f_L$, where the 'double well' and 'interpolation' functions have the forms $g(\varphi)=\frac{1}{4}\varphi^2(1-\varphi)^2$ and $p(\varphi)=\varphi^3(10-15\varphi+6\varphi^2)$, respectively, that emerge from the thermodynamically consistent formulation of the PFT,$^{(21)}$ while the Helmholtz free energy densities of the solid and liquid, f_S and f_L, are taken from the ideal or the regular solution model. These relationships result in a free energy surface that has two minima, whose relative depth depends on the temperature and composition.

Being in unstable equilibrium, the critical fluctuation (the nucleus) can be found as an extremum of this free energy functional,$^{(15-17)}$ subject to the solute conservation constraint discussed above. To impose this constraint one adds the volume integral over the solute field times a Lagrange multiplier to the free energy. The field distributions, that extremise the free energy, have to obey the appropriate Euler–Lagrange (EL) equations, which in the case of such local functional take the form

$$\frac{\delta F}{\delta\chi}=\frac{\partial\omega}{\partial\chi}-\nabla\frac{\partial\omega}{\partial\nabla\chi}=0 \tag{2}$$

where $\delta F/\delta\chi$ stands for the first functional derivative of the free energy with respect to the field χ that can be either φ or c, while ω is the total free energy density. The EL equations have to be solved assuming that unperturbed liquid exists in the far field, while, for symmetry reasons, zero field gradients exist at the centre of the fluctuations. The same solutions can also be obtained as the nontrivial time independent solution of the governing equations for field evolution.$^{(15-17)}$

Assuming spherical symmetry that is reasonable considering the low anisotropy of the crystal–liquid interface at small undercoolings, the EL equations take the following form

$$\varepsilon_\varphi^2 T\left\{\frac{\mathrm{d}^2\varphi}{\mathrm{d}r^2}+\frac{2}{r}\frac{\mathrm{d}\varphi}{\mathrm{d}r}\right\}=wTg'(\varphi)+p'(\varphi)\{f_B-f_A\} \tag{3a}$$

$$\frac{RT}{v_m}\ln\frac{c(1-c_\infty)}{c_\infty(1-c)}=(w_A-w_B)Tg+[1-p]\{\Delta f_A-\Delta f_B\} \tag{3b}$$

where $w=(1-c)w_A+cw_B$ is the free energy scale, w_i, f_i, Δf_i, and c_∞ are the free energy scale, the free energy density the free energy density difference for pure component i=A,B, and the concentration of component A far from the fluctuation, respectively. Here $'$ stands for differentiation with respect to the argument of the function. Note that Equation (3b) provides the analytic relationship $c=c(\varphi)$, thus Equation (3a) is an ordinary differential equation for $\varphi(r)$. This equation has been solved here numerically using a fourth order Runge-Kutta method. Since φ and $\mathrm{d}\varphi/\mathrm{d}r$ are fixed at different locations, the central value of φ that satisfies $\varphi\to\varphi_\infty=1$ for $r\to\infty$, has been determined iteratively. Having determined the solutions $\varphi(r)$ and $c(r)$, the work of formation of the nucleus W^* can be obtained by inserting the solution into the free energy functional. The steady state nucleation rate J_{SS} is calculated using the classical nucleation prefactor, J_0 as given by Kelton$^{(22)}$

$$J_{SS}=J_0\exp\{-W^*/kt\} \tag{4}$$

a prefactor verified experimentally on oxide glasses.$^{(23,24)}$

In the binary case the three model parameters ε_φ, w_A and w_B can be determined from the interface free energy and thickness, which are known for the equilibrium planar interface of each of the pure components. In fact, with this information the problem is over determined, thus we assign a linear temperature dependence which can be assigned to one of the model parameters, which for symmetry reasons is chosen to be the coefficient of the square gradient (SG) term, $\varepsilon_\varphi=\varepsilon_\varphi(T)$. Then, the height of the nucleation barrier can be predicted, with no fitting parameters, for all undercoolings and initial liquid compositions. It is worth noting that in the one component limit the model contains only two parameters ε_φ and w that can be fixed provided that the interface free energy and interface thickness are known for the equilibrium interface.

We use a similar approach for modelling crystal nucleation in the hard sphere system.$^{(25)}$ Here the conserved field is the volume fraction $v=\pi\sigma^3\rho/6$, where σ is the diameter of the hard spheres and ρ the number density. Owing to the complex form of $f_S(v)$ and $f_L(v)$ emerging from the equations of state fitted to molecular dynamics simulations, the respective Equation (3b) can only be inverted numerically.

Formal theory of polycrystalline solidification

Nucleation growth problems are usually handled in the framework of the Johnson–Mehl–Avrami–Kolmogorov (JMAK) approach. The 'overlapping' crystalline fraction is given by the integral

$$\zeta(t)=\frac{4\pi}{3}\int_0^t J(\tau)\left\{R^*+\int_\tau^t v(\vartheta)\,\mathrm{d}\vartheta\right\}^3\mathrm{d}\tau \tag{5}$$

where J, v and R^* are the nucleation and growth rates, and the radius of the critical fluctuation, while the integration variables ϑ and τ have time dimension. This expression coincides with the true crystalline fraction X at the beginning of the process, when the crystalline particles grow independently. However, soon they overlap, and several times covered volumes form, and Equation (5) overestimates the true crystalline fraction. A simple mean field correction $\mathrm{d}X=(1-X)\mathrm{d}\zeta$ that counts only that fraction of $d\zeta$ that falls on the untransformed region, yields $X=1-exp\{-\zeta\}$. This approach is exact if (i) the system is infinite, (ii) the nucleation rate is spatially homogeneous and (iii) either a common time dependent growth rate applies or the anisotropically growing particles are aligned parallel. Then, for constant nucleation and growth rates in infinite systems, the time evolution follows the JMAK scaling $X=1-\exp\{-(t/t_0)^p\}$, where t_0 is a time constant, $p=1+d$ is the Kolmogorov exponent and d is the number of dimensions.(26)

In systems, where chemical diffusion plays a significant role, condition (iii) is not satisfied. We are going to apply the phase field theory to explore what happens in such a case.

Phase field theory for polycrystalline solidification

Once the free energy functional is defined, crystal growth is described by the usual governing equations that ensure positive entropy production. For the nonconserved phase field, a Cahn–Allen type equation applies

$$\frac{\partial\varphi}{\partial t}=-M_\varphi\frac{\delta F}{\delta\varphi} \tag{6a}$$

while for the conserved fields a Cahn–Hilliard equation is appropriate

$$\frac{\partial c}{\partial t}=\nabla\left(M_c\nabla\frac{\delta F}{\delta c}\right) \tag{6b}$$

Here M_φ and M_c are the respective field mobilities that can be related to the kinetic coefficient of growth and the diffusion coefficient.

The phase field theory of a single crystal particle has been worked out for two and three dimensions, and with appropriate handling of the interface it reproduces the results of the microscopic solvability theory of dendritic solidification.(3,4,27,28) In this paper we work in two dimensions. We now scale the equations by a length ξ (a characteristic size) and time ξ^2/D_l yielding the dimensionless forms

$$\frac{\partial\varphi}{\partial\tilde{t}}=\left[(1-c)m_A+cm_B\right]\left\{\begin{array}{l}-\dfrac{\partial}{\partial\tilde{x}}\left(ss'\dfrac{\partial\varphi}{\partial\tilde{y}}\right)+\dfrac{\partial}{\partial\tilde{y}}\left(ss'\dfrac{\partial\varphi}{\partial\tilde{x}}\right)\\ +\tilde{\nabla}^2\varphi+(1-c)Q_A+cQ_B\end{array}\right\} \tag{7a}$$

and

$$\frac{\partial c}{\partial\tilde{t}}=\tilde{\nabla}\left\{\lambda\tilde{\nabla}c+\lambda c(1-c)\frac{v_m}{R}\left[\left(g'\delta w+p'\frac{\delta\Delta g}{T}\right)\tilde{\nabla}\varphi\right]\right\} \tag{7b}$$

where

$$Q_{A,B}=-\frac{\xi^2}{\delta_{A,B}^2}g'(\varphi)+\frac{\xi^2L_{A,B}\left(T-T_{A,B}\right)}{6\sqrt{2}\gamma_{A,B}\delta_{A,B}T}p'(\varphi)$$

$\delta w=w_B-w_A$, $\delta\Delta g=\Delta g_B-\Delta g_A$, R the gas constant, v_m the average molar volume, while m_i, L_i, T_i, δ_i and γ_i are the reduced phase field mobility, heat of fusion, melting point, interface thickness and interface free energy for the pure components (i=A and B). The quantities marked with tilde are dimensionless. The anisotropy of the interface free energy is given by the function $s=1+s_0\cos(n\vartheta)$ for n-fold symmetry, where $\vartheta=\mathrm{atan}[(\partial\varphi/\partial y)/(\partial\varphi/\partial x)]$ is the local interface orientation angle (x and y are rectangular coordinates).

To describe particles with different crystallographic orientations, the formation of grain boundaries, and grain boundary dynamics, we follow KWC,(14) and introduce an orientational field $\theta\in[0,1]$, a normalised orientation angle that gives how the crystal planes alignment in the laboratory frame (in 2D a single angle suffices to fix orientation). To recover the grain boundary dynamics inherent in their model, we add $f_{ori}=H|\nabla\theta|$ to f_S. This term is known to reproduce a rich set of behaviours including grain rotation, grain boundary wetting, etc.(29)

Unlike Kobayashi, Warren & Carter, we extend the orientation field to the liquid regions(15–17) where θ is assumed to fluctuate in space and time. Assigning local crystal orientation to liquid regions, even a fluctuating one, may seem artificial at first sight. However, due to geometrical constraints a short-range order exists even in simple liquids, which is often similar to the one in the solid. By rotating the crystalline first neighbour shell so that it matches the best to the local liquid structure, we can assign a local orientation to every atom in the liquid. This orientation fluctuates in time. The correlation of the atomic positions/angles shows how good this fit is. (In our approach the orientation field and the phase field play these roles.) Approaching the solid from the liquid, the orientation becomes more definite and matches to that of the solid, while the correlation between the local liquid structure and the crystal structure improves.

Since the orientation field is a non-conservative one, the dimensionless equation of motion is

$$\frac{\partial\theta}{\partial\tilde{t}}=\xi\chi H\tilde{\nabla}\left\{\left[1-p(\varphi)\right]K'\left(\left|\tilde{\nabla}\theta\right|\right)\frac{\tilde{\nabla}\theta}{\left|\tilde{\nabla}\theta\right|}\right\} \tag{7c}$$

where χ is the reduced orientation mobility, related to the rotational diffusion coefficient, and $K(|\nabla\theta|)=|\nabla\theta|$. Note that a term proportional to f_{ori} enters equation (7a).

According to computer simulations and real time experiments on colloidal suspensions,(30) during nucleation the crystal like clusters dynamically form and decay, and then reform again with different orientation, etc. To model this phenomenon, we introduce fluctuations of the phase and orientation fields (Langevin noise in the dynamic equations).

Equations (7) are solved by an explicit finite difference scheme on 3000×3000 and 7000×′7000 rectangular grids under periodic boundary conditions. The computer code has been parallelised using the MPI protocol. To perform the computations a PC cluster dedicated to phase field modelling has been built and housed at the Research Institute for Solid Sate Physics and Optics. Currently this cluster contains 56 nodes

Table 1. *Source of physical properties used in calculating the nucleation rate/barrier height*

	LJ	*Ice–water*	*HS*
Thermodyn.	31	32	33
δ	34	35	36,37
γ	38	39	40
D_l	31	32	
J_{SS}	41	42,43	

of 1 to 2·4 GHz Athlon processors.

This model can also be extended to describe eutectic/peritectic solidification where the two phases have the same structure (e.g. Ag–Cu, Ag–Pt). This is realised by incorporating regular solution thermodynamics, a SG term for the chemical composition (a fourth order differential operator appears then in Equation (7b)), while a more complex form of K is used that sets preference for a definite orientational relationship between the two solid phases α and β: $K(c,|\nabla\theta|, |\nabla\theta|^2)$, where $K=h(c)K_1(|\nabla\theta|)+[1-h(c)]K_2(|\nabla\theta|)+{}^1/_2\varepsilon_\theta{}^2TH^{-1}|\nabla\theta|^2$, and we use the following functions

$$h(c)={}^1/_2\{1+\cos[(c-c_\alpha)/(c_\beta-c_\alpha)2\pi]\}$$

$$K_1(|\nabla\theta|)=|\nabla\theta|$$

$$K_2(|\nabla\theta|)=a+b|\cos(2n\pi d|\nabla\theta|+\psi)|$$

Here c_α and c_β are the equilibrium solid compositions, a and b are constants, d is the interface thickness, while n, or ψ, or both can be used to define the preferred orientation change at the interface. Note that the function $h(c)$ controls the preference for the orientation change for solid compositions that differ significantly from the equilibrium solid compositions $c_\alpha<c<c_\beta$. Such intermediate compositions normally occur only at the α–β interface in the solid. Anisotropy of the free energy of the phase boundary might be incorporated by making either $\varepsilon_\theta{}^2$ or ψ dependent on the interface inclination angle $\vartheta_c=a\tan[(\partial c/\partial y)/(\partial c/\partial x)]$. While the functions used here have been chosen intuitively, for different combinations of crystal structures, K_1 and K_2 can be deduced on physical grounds.

Material parameters

The nucleation studies were performed for the Lennards–Jones (LJ), ice–water, and hard sphere (HS) systems. In all these cases the thermodynamic and interfacial properties are available from sources specified in Table 1. Thus the calculations can be made without adjustable parameters, and can be compared with nucleation rates from simulations or experiment, or with the height of the nucleation barrier from simulations, Table 1.(31–44)

The phase field simulations for polycrystalline solidification of a single crystalline phase were performed using the properties of the Cu–Ni system given in Table 2. Since the physical thickness of the interface is in the nanometer range and the typical solidification structures are far larger (μm to mm), a full simulation of polycrystalline solidification from nucleation to particle impingement cannot be performed even with the fastest of the present supercomputers. Therefore, following other authors,(5,6) the interface thickness has been increased by a factor of 20, the interface free energy has been divided by 6, while the diffusion coefficient has been increased by a factor of 100. This allows us to follow the life of crystallites from birth to impingement on each other. The time and spatial steps were $\Delta t=4{\cdot}75\times10^{-6}$ and $\Delta x=6{\cdot}25\times10^{-3}$, $\xi=2{\cdot}1\times10^{-4}$ cm and $D_l=10^{-5}$ cm²/s. Dimensionless mobilities of $\xi^2M_\varphi/D_l=0{\cdot}9$, $\xi M_{\theta,1}H/D_l=720$ and $\xi M_{\theta,1}H/D_l=7{\cdot}2\times'10^{-4}$ were applied, while $D_l=0$ was taken in the solid. The simulations were performed at 1574 K for various reduced liquid composition $x=(c_\infty-c_s)/(c_l-c_s)$ between the solidus and liquidus, where $c_s=0{\cdot}399112$ and $c_l=0{\cdot}466219$ are the solidus and liquidus compositions. White noises of amplitudes 0·0025, 0 and 0·25 were used for the three fields φ, c and θ, respectively.

Table 2. *Physical properties of Cu, Ni and Ag used in phase field simulations*

	Cu	*Ni*	*Ag*
T_f (K)	1358	1728	1234
L (J/cm³)	1728	2350	1097
γ (mJ/m²)	247	315	140
D_l (cm²/s)	10^{-5}	10^{-5}	10^{-5}

In the case of eutectic solidification of the Ag–Cu system at T=900 K the interaction parameters are chosen so that the respective phase diagram approximates reasonably the experimental one [$\Omega_Lv=(16000-4T)$J/mol; $\Omega_Sv=(26000-4T)$ J/mol]. At this temperature the equilibrium solid concentrations are $c_\alpha\approx0{\cdot}1$, and $c_\beta\approx0{\cdot}9$, while the eutectic concentration is ~0·35. The dimensionless time and spatial steps we use are $2{\cdot}5'\times10^{-7}$, and 5×10^{-3}, while $\xi=6'\times10^{-6}$ cm. The simulations were performed on a 1000×′1000 grid. With an appropriate choice of the parameters $a=0{\cdot}9/d$, $b=0{\cdot}1/d$, $n={}^1/_2$, $\psi=0$, $d=\Delta x$, $\zeta_c=1$, $\zeta_\theta=(\varepsilon_\theta/\varepsilon_\varphi)^2=10^{-9}$, where ε_θ is the SG term for concentration, we are able to simulate multigrain eutectic solidification. Note that the choice $n=0{\cdot}5$ gives preference to a step of $\Delta\theta=\pm0{\cdot}5$ in the orientation field at the α–β interface. Consequently, a particle of the dominant phase of orientation θ prefers contact with a grain of the secondary crystalline phase of orientation $\theta'=\theta+\Delta\theta$.

Results

Prediction of nucleation barrier in 3D

The nucleation rates predicted for the LJ and ice–water systems by the phase field theory are compared

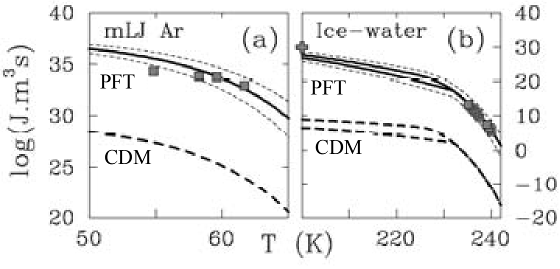

Figure 1. *Nucleation rate versus temperature as predicted for (a) the Lennard–Jones and (b) the ice–water systems by the phase field theory (PFT, solid line) and by the classical droplet model (CDM, dashed line). The dotted lines above and below the PFT results show the uncertainty originating from the error of the interface free energy. For comparison results from molecular dynamics(41) and experiment(42,43) are also shown*

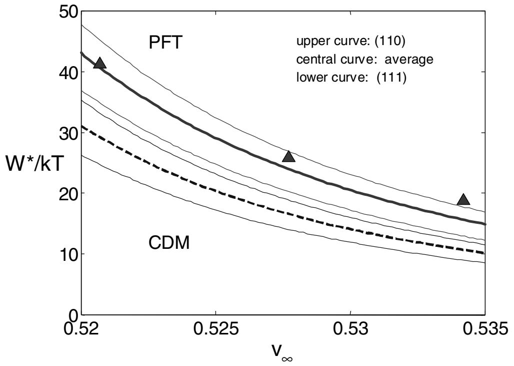

Figure 2. *Reduced nucleation barrier height versus volume fraction of the initial liquid. [Upper three lines (solid): phase field theory - PFT; lower three lines (dashed/dotted): classical droplet model - CDM.] Within these triplets of lines for PFT and CDM, the upper and lower curves were calculated using the physical properties of the (110) and (111) interfaces, respectively (as indicated by the caption in the figure). The prediction for the (100) interface (not shown here) falls slightly below the results obtained with the average interface properties (heavy lines). For comparison, the results of Monte Carlo simulations(44) are also shown (triangles)*

with the results of computer simulations and measurements in Figure 1. Note that these predictions are made without adjustable parameters. The nucleation rates from the PFT are in a reasonable agreement with the simulations and the experiments.(15–17) This success of the PFT follows from two sources. (i) The realistic temperature dependence of the equilibrium interface free energy it predicts, namely $\gamma_{eq} \propto T$; this relationship is trivially satisfied for the HS system and is also followed by other simple liquids, as shown by recent MD simulations for the Lennard–Jones system.(45) (ii) The ability to work with local properties that differ from the bulk ones. Indeed, under the conditions of interest, no bulk properties have been seen even at the centres of the critical fluctuations. Accordingly, the classical sharp interface droplet model, which relies on bulk thermodynamic properties and the value of the interface free energy taken at the melting point, underestimates the nucleation rate by 10 to 20 orders of magnitude.

Similar results were obtained using our two-order-parameter PFT for crystal nucleation in the HS liquid.(25) The interface thickness for phase field is evaluated from the cross-interfacial variation of the height of the singlet density peaks given in Refs 36 and 37. The model parameters are fixed in equilibrium so that the free energy and thickness of the (111), (110) and (100) interfaces from molecular dynamics are recovered. The density profiles predicted without adjustable parameters are in a good agreement with the filtered densities(36,37) from the simulations. The barrier heights calculated with the properties of the (111) and (110) interfaces envelope the Monte Carlo results,(44) while those obtained with the average interface properties fall very close to the exact values. As pointed out previously,(44) the sharp interface droplet model considerably underestimates the height of the nucleation barrier, which leads to a 3 to 5 orders of magnitude difference in the nucleation rate.

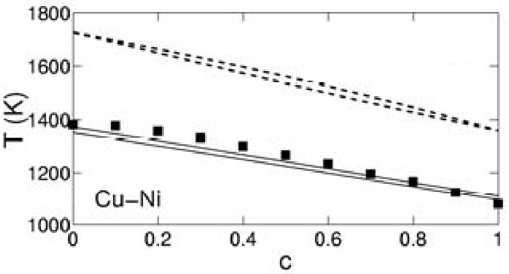

Figure 3. *Nucleation temperature versus composition predicted by the phase field theory for the nearly ideal Cu–Ni system. Upper and lower solid lines correspond to nucleation rates of 10^{-4} to 1 drop^{-1}s^{-1} for droplets of 6 mm diameter. The experimental data (squares) refer to electromagnetically levitated droplets.(46) The calculated liquidus and solidus lines (dashed) are also shown*

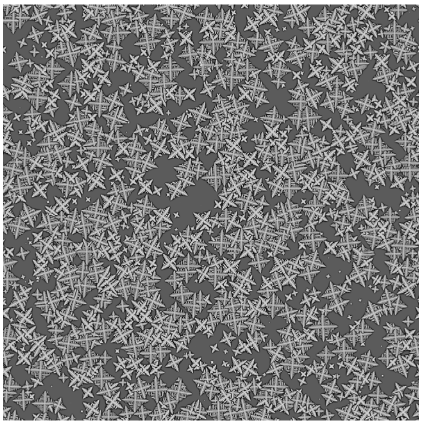

Figure 4. *Solidification morphology for primary crystallisation in a binary alloy (Ni–Cu) at 1574 K, and supersaturation 0·8. By the end of solidification ~1460 dendritic particles form. The calculations were performed on a 7000×7000 grid*

In the case of binary alloys, such a rigorous test cannot be performed since the input information available for the crystal–liquid interface is far less reliable. In the nearly ideal Cu–Ni system, the critical undercoolings computed for a realistic range of nucleation rates (J=10^{-4} to 1 drop^{-1} s^{-1} for electromagnetically levitated droplets of 6 mm diameter) fall close to the experimental values(46) (see Figure 3). This indicates a homogeneous nucleation, contradicting thus the heterogeneous mechanism suggested earlier(46) on the basis of Spaepen's value α_{HS}=0·86(47) for the dimensionless interfacial free energy of the HS system. (Note that $\alpha=\gamma N_0^{1/3} v_m^{2/3}/\Delta H_f$, where N_0 is the Avogadro number.) Recent computer simulations yield considerably smaller values α_{HS}=0·51(40) and α_{Ni}=0·58(48) (close to the 0·6 we used), invalidating the earlier conclusion. These findings raise the possibility that homogeneous nucleation is more common in alloys than previously thought.

Transformation kinetics in 2D

A snapshot of polycrystalline dendritic solidification in the phase field theory, for the Cu–Ni system at 1574 K in 2D is shown in Figure 4. The large number of particles (~1500) provides reasonable statistics to evaluate the Kolmogorov exponent p.

We compare four simulations: two are performed for a reduced concentration of x=0·2, while the others at 0·5 and 0·8. 1000×1000 sections of the respective

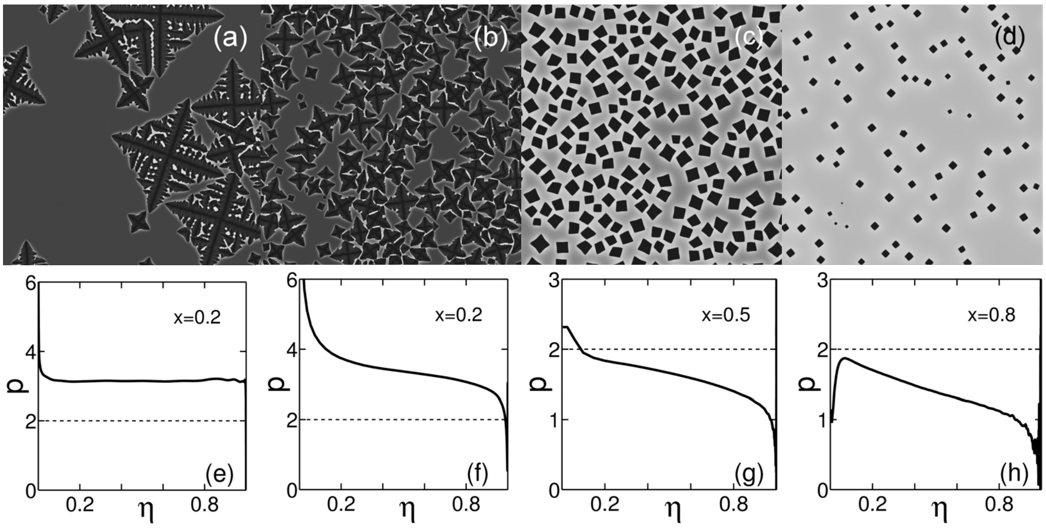

Figure 5. *Transformation kinetics in 2D versus composition in the Cu–Ni system at 1574 K. (a)–(d) Snapshots of the concentration distribution (black – solidus; light gray – liquidus); and the respective Kolmogorov exponent vs normalised transformed fraction curves are shown. Simulations presented in panels (a) and (b) differ in the magnitude of the nucleation rate*

simulations are shown in Figure 5 (panels (a)–(d)), together with the respective Kolmogorov exponents evaluated as a function of the normalised crystalline fraction $\eta=X/X_{\mathrm{max}}$, (panels (e)–(h)), where X_{max} is the maximum crystalline fraction achievable at the given liquid composition. If the nucleation rate is sufficiently low there is space enough to develop a full dendritic morphology, Figure 5(a). Since the dendrite tip is a steady state solution of the diffusion equation, constant nucleation and growth rates apply, that are expected to yield $p=1+d$.(26) Indeed, the observed Kolmogorov exponent is $p\approx3$. In the other simulations, the particles have a more compact shape, and interact via their diffusion fields, a phenomenon known as 'soft impingement'. The respective Kolmogorov exponents decrease with increasing solid fraction. A closer inspection of the process indicates that growth in the initial stage after nucleation is interface controlled (governed by the phase field mobility), as opposed to control by chemical diffusion. This results in a delay in the onset

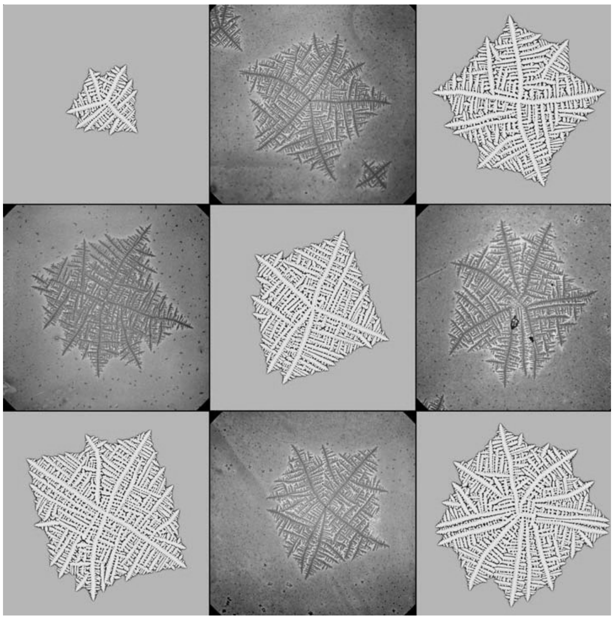

Figure 6. *'Dizzy' dendrites formed by sequential deflection of dendrite tips on foreign particles: comparison of experiments on 80 nm clay-polymer blend film (dark gray panels, by the courtesy of V. Ferreiro and J. F. Douglas, for experimental details see Refs 50,51) and phase field simulations (light gray panels). The simulations have been selected from 30 random configurations according to their resemblance to the experimental patterns. (The simulations were performed on a 3000×3000 grid, with 18000 orientation pinning centres per frame)*

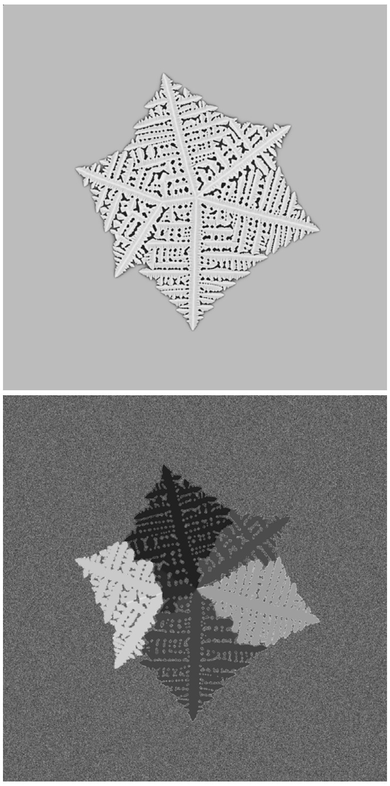

Figure 7. *Disordered dendrite formed by dynamic trapping of orientation defects, which initiated the growth of new grains (left: composition map; right: orientation map) as predicted by the phase field theory*

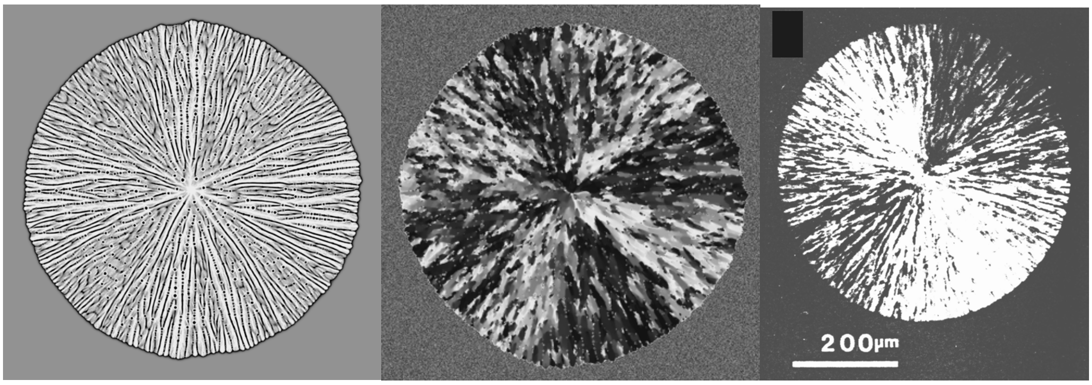

Figure 8. *Polycrystalline spherulites formed in phase field simulations (left: composition map; centre: orientation map) and in experiment (right panel, courtesy of G. Ryschenkow & G. Faivre, for details see Ref. 53)*

of diffusion controlled growth, which will lead to a *p* decreasing with time. Such an effect will only be perceptible in the case of copious nucleation, where the length of this transient period is comparable to the total solidification time. Indeed, similar behaviour has been observed during the formation of nanocrystalline materials when crystallising metallic glass ribbons.(49)

Polycrystalline growth morphologies in 2D

In thin polymer blend films crystallisation morphology can be influenced spectacularly by adding foreign (clay) particles.(50,51) This leads to the formation of disordered dendritic structures ('dizzy' dendrites), see Figure 6. These structures are formed by the engulfment of the clay particles into the crystal, inducing the formation of new grains. This phenomenon is driven by the impetus to reduce the crystallographic misfit along the perimeter of clay particles by creating grain boundaries within the polymer crystal. This process changes the crystal orientation at the dendrite tip, changing thus the tip trajectory ('tip deflection'). To model this, we introduced randomly distributed 'orientation pinning centres' to the simulation which are represented by regions of externally imposed orientation.(18) Since relevant material properties are unknown for the polymer mixtures, the computations were performed for the familiar Ni/Cu system, which, as is the case with polymers, is both miscible and forms nearly square crystals close to equilibrium.

Our simulations show that tip deflection happens only when the pinning centre is above a critical size, comparable to the dendrite tip radius. Pinning centres cause deflection only if directly hit by the dendrite tip, a finding confirmed by experiment. This explains why only a small fraction of the pinning centres influence morphology. Using an appropriate density of pinning centres comparable to the density of clay particles, a striking similarity is obtained between experiment and simulation, Figure 6. This extends to such details as curling of the main arms and the appearance of extra arms. This disorder in dendrite morphology originates from a polycrystalline structure that develops during a sequential deflection of dendrite tips on foreign particles.(18)

Another way to form polycrystalline growth morphologies is via reducing the orientational mobility. Below a critical M_θ, a uniform orientation cannot be established along the whole perimeter of the crystalline particles, polycrystalline grains form due to the orientational disorder quenched in. At anisotropies that lead to the formation of dendritic particles, reduced M_θ leads to the formation of 'dizzy' dendrites without foreign particles, Figure 8. Here the dynamically entrapped orientational disorder is responsible for the polycrystalline structure. This route to form 'dizzy' dendrites is yet to be confirmed experimentally.

Both in experiment and phase field simulations, at

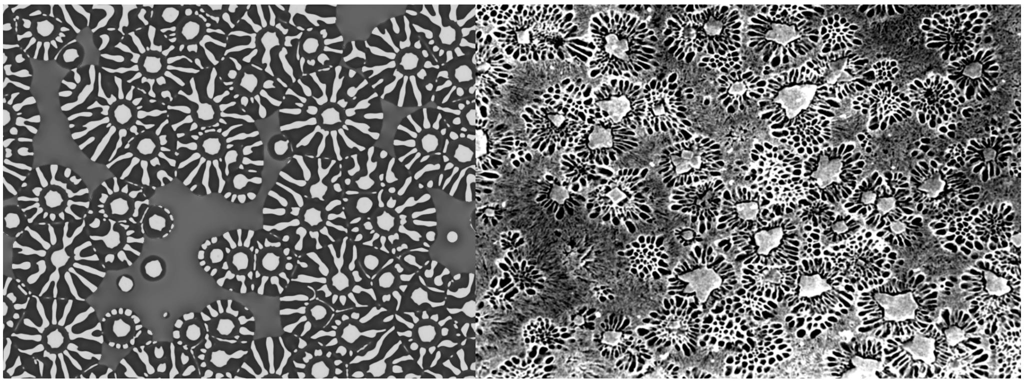

Figure 9. *Flowerlike eutectic spherulites formed in phase field simulations (left) and in a laser melted Al–Si alloy (right, by the courtesy of J. H. Perepezko). For the experimental details see Ref. 54*

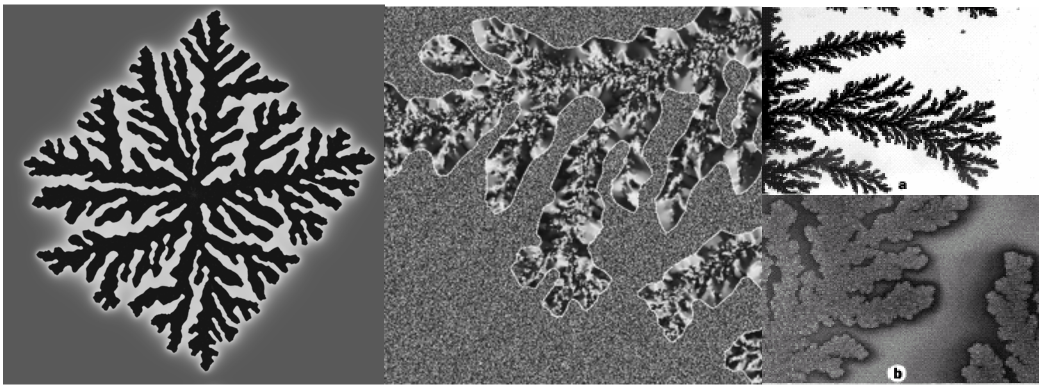

Figure 10. *Polycrystalline aggregates formed in phase field simulations (left: composition map; center: orientation map) and in electrodeposition experiment (rightmost panels; (a) and (b) show different magnifications; by the courtesy of V. Fleury, for details see Ref. 56)*

large supersaturations, space filling multigrain objects appear, the well known polycrystalline spherulites(52) (Figure 8) that are composed of radially elongated grains.(17,53) They form if only the long range chemical diffusion is negligible. This occurs when the solute is trapped either in the solid, in liquid inclusions (droplets or channels) or in a second solid phase of higher solute concentration (eutectic spherulites, Figure 9).(54,55)

Polycrystalline fractal like particle aggregates form if the solidification is diffusion controlled and the orientational mobility is low,Figure 10. These morphologies are similar to those seen in diffusion limited aggregation, and resemble closely to the fractal like polycrystalline aggregates seen in electro-deposition.(56)

Summary

We have shown for the Lennard–Jones, ice–water, and hard sphere systems, that using accurate interfacial properties to fix the model parameters, the phase field theory can be made quantitative: one can predict the nucleation rate and nucleation barrier height with good accuracy. In contrast, the classical droplet model predicts nucleation rates that differ from the true values by several orders of magnitude.

From large scale phase field simulations, which rely on an orientation field in handling nucleation and anisotropic growth with different crystallographic orientations, we determined the Kolmogorov exponent for polycrystalline dendritic solidification and for the ‘soft impingement’ of compact particles interacting via their diffusion fields. The Kolmogorov exponents obtained agree with theoretical expectations and experiments.

The same theory has been used to model the formation of polycrystalline growth morphologies via incorporating static and dynamic heterogeneities (foreign particles and orientational defects frozen in the crystal due to the reduced orientational mobility, respectively). We demonstrated that the present approach can be used to model the formation of a broad variety of polycrystalline morphologies, including disordered dendrites, spherulites and fractal like aggregates.

Acknowledgments

We thank R. L. Davidchack and B. B. Laird for communicating to us their new high resolution density data for the Lennard–Jones system prior to publication. We thank V. Ferreiro, J. F. Douglas, G. Faivre, J. H. Perepezko and V. Fleury for the experimental pictures on polycrystalline growth morphologies. This work has been supported by the European Space Agency under Prodex Contract Nos. 14613/00/NL/SFe and 90109, the Hungarian Academy of Sciences under contract No. OTKA-T-037323 and by the Norwegian Research Council under project Nos. 153213/432 and 151400/210.

References

1. Boettinger, W. J., Warren, J. A, Beckermann, C. & Karma, A. Phase field simulation of solidification. *Ann. Rev. Mater. Res.*, 2002, **32**, 163–94.
2. Kobayashi, R. Modeling and numerical simulation of dendritic crystal growth. *Physica D*, 1993, **63**, 410–23.
3. Karma, A. & Rappel, W.-J. Quantitative phase-field modeling of dendritic growth in two and three dimensions. *Phys. Rev. E*, 1998, **57**, 4323–49.
4. Bragard, J., Karma, A., Lee, Y. H. & Plapp, M. Linking phase-field and atomistic simulations to model dendritic solidification in highly undercooled melts. *Interface Sci.*, 2002, **10**, 121–6.
5. Warren, J. A. & Boettinger, W. J. Prediction of dendritic growth and micro- segregation patterns in a binary alloy using the phase-field method. *Acta Metall. Mater.*, 1995, **43**, 689–703.
6. Conti, M. Growth of needle crystal from an undercooled alloy melt. *Phys. Rev. E*, 1997, **56**, 3197–202.
7. George, W. L. & Warren, J. A. A parallel 3D dendritic growth simulator using the phase-field method. *J. Comput. Phys.*, 2002, **177**, 264–83.
8. Karma, A. Phase-field model of eutectic growth. *Phys. Rev. E*, 1994, **49**, 2245–50.
9. Elder, K. R., Drolet, F., Kosterlitz, J. M. & Grant, M. 1994 Stochastic eutectic growth. *Phys. Rev. Lett.*, 1994, **72**, 677–80.
10. Nestler, B. & Wheeler, A. A. A multi-phase-field model of eutectic and peritectic alloys: Numerical simulation of growth structures. *Physica D*, 2000, **138**, 114–33.
11. Lo, T. S., Karma, A. & Plapp, M. Phase-field modeling of microstructural pattern formation during directional solidification of peritectic alloys without morphological instability. *Phys. Rev. E*, 2001, **63**, 031504–1–15.
12. Drolet, F., Elder, K. R., Grant, M. & Kosterlitz, J. M. Phase-field modeling of eutectic growth. *Phys. Rev. E*, 2000, **61**, 6705–20.
13. Simmons, J. P., Shen, C. & Wang, Y. Phase field modeling of simulataneous nucleation and growth by explicitly incorporating nucleation events. *Scripta Mater.*, 2000, **43**, 935–42.
14. Kobayashi, R., Warren, J. A. & Carter, W. C. Vector-valued phase field model for crystallization and grain boundary formation. *Physica D*, 1998, **119**, 415–23.
15. Gránásy, L., Börzsönyi, T. & Pusztai, T. Crystal nucleation in binary phase-field theory. *J. Cryst. Growth.*, 2002, **237–239**, 1813–17.
16. Gránásy, L., Börzsönyi, T. & Pusztai, T. Nucleation and bulk crystallization in binary phase field theory. *Phys. Rev. Lett.*, 2002, **88**, 206105–1–4.
17. Gránásy, L., Börzsönyi, T. & Pusztai, T. Phase field theory of nucleation and growth in binary alloys. In *Interface and transport dynamics, computational modelling*. Volume 32. Edited by H. Emmerrich, B. Nestler, & M. Schreckenberg. Lecture Notes in Computational Science and Engineering. Springer, Berlin, 2003. Pp 190–5.
18. Gránásy, L., Pusztai, T., Douglas, J. F., Warren, J. A., Börzsönyi, T. &

Ferreiro, V. Growth of 'dizzy dendrites' in a random field of foreign particles. *Nature Mater.*, 2003, **2**, 92–6.

19. Caginalp, G. & Jones, J. A derivation and analysis of phase field models of thermal alloys. *Ann. Phys. NY*, 1995, **237**, 66–107.
20. Shen, Y. C. & Oxtoby, D. W. Nucleation of Lennard-Jones fluids: a density functional approach. *J. Chem. Phys.*, 1996, **105**, 6517–24.
21. Wang, S. L., Sekerka, R. F., Wheeler, A. A., Murray, B. T., Coriell, S. R., Braun, R. J. & McFadden, G. B. Thermodynamically-consistent phase-field models for solidification. *Physica D*, 1993, **69**, 189–200.
22. Kelton, K. F. Crystal nucleation in liquids and glasses. *Solid State Phys.*, 1991, **45**, 75–177.
23. Kelton, K. F. & Greer, A. L. Test of classical nucleation theory in glasses. *Phys. Rev. B*, 1988, **38**, 10089–92.
24. Greer, A. L. & Kelton, K. F. Nucleation in lithium-disilicate glass: a test of classical theory by quantitative modeling. *J. Am. Ceram. Soc.*, 1991, **74**, 1015–22.
25. Gránásy, L., Pusztai, T., Tóth, G., Jurek. Z., Conti, M. & Kvamme, B. Phase field theory of crystal nucleation in hard sphere liquid. *J. Chem. Phys.* 2003, **119**, 10376–82.
26. Christian, J. W. *The theory of transformations in metals and alloys*. 1981. Pergamon, Oxford.
27. Karma, A. & Rappel, W.-J. Phase-field method for computationally efficient modeling of solidification with arbitrary interface kinetics. *Phys. Rev. E*, 1996, **53**, R3017–20.
28. Karma, A. Phase-field formulation for quantitative modeling of alloy solidification. *Phys. Rev. Lett.*, 2001, **87**, 115701–1–4.
29. Kobayashi, R., Warren, J. A. & Carter, W. C. Modeling grain boundaries using a phase-field technique. *Physica D*, 2000, **140**, 141–50.
30. Gasser, U., Weeks, E. R., Schofield, A., Pusey, P. N. & Weitz, D. A. Real-space imaging of nucleation and growth in colloidal crystallization. *Science*, 2001, **292**, 258–62.
31. Broughton, J. Q. & Gilmer, H. H. Molecular dynamics investigation of the crystal-fluid interface. I. Bulk properties. *J. Chem. Phys.*, 1983, **79**, 5095–104.
32. Gránásy, L. Cahn-Hilliard-type density functional calculations for homogeneous ice nucleation in undercooled water. *J. Molec. Struct.*, 1999, **485–486**, 523–36.
33. Hall, K. R. Another hard-sphere equation of state. *J. Chem. Phys.*, 1970, **57**, 2252–4.
34. Laird, B. B. & Haymet, A. D. J. The crystal/liquid interface: Structure and properties from computer simulations. *Chem. Rev.*, 1992, **92**, 1819–37.
35. Hayward, J. A. & Haymet, A. D. J. The ice/water interface: Molecular dynamics simulations of the basal, prism, (2021), and (2110) interfaces of ice Ih. *J. Chem. Phys.*, 2001, **114**, 3713–26.
36. Davidchack, R. L. & Laird, B. B. Simulation of the hard-sphere crystal-melt interface. *J. Chem. Phys.*, 1998, **108**, 9452–62.
37. We received new, high-resolution density data for the (111), (110), and (100) interfaces from R. L. Davidchack and B. B. Laird. They are fully consistent with their previous results for the (100) and (111) interfaces, published in Ref. 36.
38. Broughton, J. Q. & Gilmer, H. H. Molecular dynamics investigation of the crystal-fluid interface. VI. Excess surface free energies of crystal-liquid systems. *J. Chem. Phys.*, 1986, **84**, 5759–68.
39. Hardy, S. C. Grain-boundary groove measurement of surface-tension between ice and water. *Phil. Mag.*, 1977, **35**, 471–84.
40. Davidchack, R. L. & Laird, B. B. Direct calculation of the hard-sphere crystal/melt interfacial free energy. *Phys. Rev. Lett.*, 2000, **85**, 4751–4.
41. Báez, L. A. & Clancy, P. The kinetics of crystal growth and dissolution from the melt in Lennard-Jones systems. *J. Chem. Phys.*, 1995, **102**, 8138–48.
42. Taborek, P. Nucleation in emulsified water. *Phys. Rev. B*, 1985, **32**, 5902–6.
43. Huang, J. & Bartell, L. S. Kinetics of homogeneous nucleation in the freezing of large water clusters. *J. Phys. Chem.*, 1995, **99**, 3924–31.
44. Auer, S. & Frenkel, D. Prediction of absolute crystal-nucleation rate in hard-sphere colloids. *Nature*, 2001, **409**, 1020–3.
45. Davidchack, R. L. & Laird, B. B. Direct calculation of the crystal-melt interfacial free energies for continuous potentials: Application to the Lennard-Jones system. *J. Chem. Phys.* 2003, **118**, 7651–7.
46. Willnecker, R., Herlach, D. M. & Feuerbacher, B. Nucleation in bulk undercooled nickel-based alloys. *Mater. Sci. Eng.*, 1988, **98**, 85–8.
47. Spaepen, F. & Meyer, R. B. Surface-tension in a structural model for solid-liquid interface. *Scripta Metall.*, 1976, **10**, 257–63.
48. Hoyt, J. J., Asta, M. & Karma, A. Method for computing the anisotropy of the solid-liquid interfacial free energy. *Phys. Rev. Lett.*, 2001, **86**, 5530–3.
49. Pradell, T., Crespo, D. Clavaguera, N. & Clavaguera-Mora, M. T. Diffusion controlled grain growth in primary crystallization: Avrami exponents revisited. *J. Phys.: Condens. Matter*, 1998, **10**, 3833–44.
50. Ferreiro, V., Douglas, J. F., Warren, J. A. & Karim, A. Nonequilibrium pattern formation in the crystallization of polymer blend films. *Phys. Rev. E*, 2002, **65**, 042802–1–4.
51. Ferreiro, V., Douglas, J. F., Warren, J. A. & Karim, A. Growth pulsations in symmetric dendritic crystallization in polymer blend films. *Phys. Rev. E*, 2002, **65**, 051606–1–16.
52. Keith, H. D. & Padden, F. J., Spherulitic crystallization from the melt. I. Fractional and impurity segregation and their influence on crystalline morphology. *J. Appl. Phys.*, 1964, **35**, 1270–85.
53. Ryschenkow, G. & Faivre, G. Bulk crystallization of liquid selenium–primary nucleation, growth-kinetics and modes of crystallization. *J. Cryst. Growth*, 1988, **87**, 221–35.
54. Gremaud, M., Allen, D. R., Rappaz, M. & Perepezko, J. H. The development of nucleation controlled microstructures during laser treatment of Al-Si alloys. *Acta Mater.*, 1996, **44**, 2669–81.
55. Warren, J. A., Loginova, I., Gránásy, L., Börzsönyi, T. & Pusztai, T. Phase field modeling of alloy polycrystals. *Proc. Modeling of Casting, Welding and Advanced Solidification Processes*. 2003. Edited by D. Stefanescu *et al*. TMS Publications. Pp 45–52.
56. Fleury, V. Branched fractal patterns in non-equilibrium electrochemical deposition from oscillatory nucleation and growth. *Nature*, 1997, **390**, 145–8.